Chemical Engineering Journal 358 (2019) 160–169

Contents lists available at ScienceDirect

Chemical Engineering Journal

journal homepage: www.elsevier.com/locate/cej

Effect of pore size distribution and particle size of porous metal oxides on phosphate adsorption capacity and kinetics

Prashanth Suresh Kumar[a,b], Leon Korving[a,*], Karel J. Keesman[a,c], Mark C.M. van Loosdrecht[b], Geert-Jan Witkamp[b,1]

[a] Wetsus, European Centre of Excellence for Sustainable Water Technology, Oostergoweg 9, 8911 MA, Leeuwarden, The Netherlands
[b] Department of Biotechnology, Applied Sciences, Delft University of Technology, Building 58, Van der Maasweg 9, 2629 HZ Delft, The Netherlands
[c] Biobased Chemistry and Technology, Wageningen University, Bornse Weilanden 9, 6708 WG, Wageningen, The Netherlands

HIGHLIGHTS

- FSP and DD6 had higher fraction of pores > 10 nm compared to GEH and CFH.
- All adsorbents showed similar adsorption capacities at equilibrium.
- Small particles of all adsorbents reached equilibrium within 7 days.
- Large particles of GEH and CFH took between 60 and 90 days reach equilibrium.
- Pores > 10 nm were important to enhance adsorption kinetics.

GRAPHICAL ABSTRACT

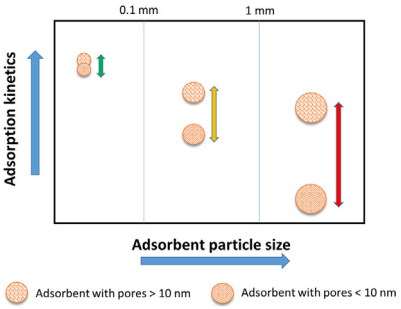

ARTICLE INFO

Keywords:
Phosphate adsorption
Particle size
Pore size distribution
Adsorption kinetics
Diffusion
Porous metal oxide

ABSTRACT

Phosphate is a vital nutrient but its presence in surface waters even at very low concentrations can lead to eutrophication. Adsorption is often suggested as a step for reducing phosphate down to very low concentrations. Porous metal oxides can be used as granular adsorbents that have a high surface area and hence a high adsorption capacity. But from a practical point of view, these adsorbents also need to have good adsorption kinetics. The surface area of such adsorbents comes from pores of varying pore size and the pore size distribution (PSD) of the adsorbents can affect the phosphate adsorption kinetics. In this study, the PSD of 4 different adsorbents was correlated with their phosphate adsorption kinetics. The adsorbents based on iron and aluminium (hydr)oxide were grinded and the adsorption performance was studied as a function of their particle size. This was done to identify diffusion limitations due to the PSD of the adsorbents. The phosphate adsorption kinetics were similar for small particles of all the adsorbents. For larger particles, the adsorbents having pores larger than 10 nm (FSP and DD6) showed faster adsorption than adsorbents with smaller pores (GEH and CFH). Even though micropores (pores < 2 nm) contributed to a higher portion of the adsorbent surface area, pores bigger than 10 nm were needed to increase the rate of adsorption.

* Corresponding author at: Wetsus, European Centre of Excellence for Sustainable Water Technology, Oostergoweg 7, 8911 MA, Leeuwarden, The Netherlands.
E-mail address: psureshkumar@tudelft.nl (L. Korving).
[1] Current address: King Abdullah University of Science and Technology (KAUST), Water Desalination and Reuse Center (WDRC), Division of Biological and Environmental Science and Engineering (BESE), Thuwal 23955-6900, Saudi Arabia.

https://doi.org/10.1016/j.cej.2018.09.202
Received 28 July 2018; Received in revised form 24 September 2018; Accepted 26 September 2018
Available online 27 September 2018

1. Introduction

Phosphate is a vital nutrient that is essential for life. It is a key component added in fertilizers for food production and has no substitute [1,2]. But concentrations of phosphate in surface waters even in the range of 0.01–0.1 mg P/L can lead to eutrophication [3,4]. This can happen via discharge from diffuse sources such as agricultural run-offs or point sources such as municipal wastewater treatment plants [5,6]. Eutrophication poses a large risk to the ecosystem resulting in environmental as well economical damage [7–9]. Hence there is a need for technology that can effectively reduce the phosphate to concentrations in the sub microgram levels.

Adsorption is often suggested as polishing technology for reducing contaminants to such low concentrations [10–12]. A chief characteristic while developing adsorbents is to improve the adsorption capacity, i.e. the amount of phosphate removed per mass of adsorbent. Since adsorption is a surface reaction, a high surface area is often seen as an important characteristic to improve the adsorption capacity [13,14]. Some studies report high capacity phosphate adsorbents by using nanoparticles which have a high surface area [15–17]. But such adsorbents are difficult to apply from a practical viewpoint due to difficulty in recovery or pressure drop related problems. These problems are overcome by immobilizing adsorbent particles in high surface area granular backbones [18–20]. Another way is to use granular porous metal oxides, where the pores give rise to a high surface area [11,21,22]. The surface area of such porous metal oxides are contributed by pores of varying size. Depending on the size of the pores as well as their arrangement, their accessibility by phosphate molecules could be affected. Moreover, the diffusion of phosphate into such pores could also get affected, which in turn will affect the adsorption kinetics. In this study, we address the effect of adsorbent pore size distribution (PSD) on the accessibility as well as diffusion of phosphate ions.

Four different granular porous metal oxide adsorbents were tested for phosphate adsorption. Three of them are based on iron oxides, namely: granular ferric hydroxide (GEH), FerroSorp Plus (FSP), compacted ferric (hydr)oxides (CFH). The other adsorbent, called DD6, is based on aluminium oxides. These adsorbents have been studied due to their varying PSD and because iron and aluminium (hydr)oxides are known for their good phosphate adsorption properties. These adsorbents have different chemical properties owing to the difference in their metal oxide composition. The type of metal oxide varies its properties like crystallinity, type and amount of surface functional groups, surface charge [23–25]. Hence the differences in phosphate adsorption from such adsorbents cannot be related directly to the PSD. To overcome this challenge, the different adsorbents were grinded to varying particle sizes of 0–0.1 mm, 0.4–0.5 mm and 1–1.25 mm. Grinding porous adsorbents does not significantly influence their surface area since a majority of their area comes from pores smaller than 50 nm, which are way smaller than the particle size (Table S1 in supporting information). In such a case, reducing the particle size will mainly reduce the path length for diffusion inside the adsorbent [26,27]. Hence by comparing adsorption performance between the different particle sizes of the same adsorbent, the effect due to chemical properties and surface area is excluded and the difference in adsorption is only due to diffusion limitation, which can be directly correlated with the PSD.

The aim of this study is to give insights on the optimum PSD that can provide accessible surface area and faster diffusion for phosphate adsorption. This will thus help in designing an adsorbent that has a high phosphate adsorption capacity along with good adsorption kinetics.

2. Materials and methods

2.1. Chemicals

Potassium dihydrogen phosphate (KH_2PO_4), hydrochloric acid (HCl) and sodium hydroxide (NaOH) were obtained from VWR chemicals. MOPS (3-(N-morpholino)propanesulfonic acid) was purchased from Sigma Aldrich. Granular ferric hydroxide (GEH), Ferrosorp Plus (FSP), compacted ferric hydroxide (CFH) were provided by GEH Wasserchemie Gmbh, HeGO Biotech Gmbh and Kemira, respectively. DD6 was purchased from BASF.

2.2. Phosphate adsorption kinetic experiments

The different adsorbents were grinded and sieved to give 3 particle size ranges: 0–100 μm, 400–500 μm, 1–1.25 mm. Aqueous solution of phosphate with a concentration of 25 mg P/L was prepared in MilliQ water. MOPS has been known to be a non-chelating agent and hence was used as the buffering agent [28]. A concentration of 20 mM of MOPS was used and the solution pH was adjusted to 7.2 with HCl and/or NaOH. The adsorbent dose was 0.2 g (dry weight) in 100 ml phosphate solutions, resulting in adsorbent concentration of 2 g/L. The adsorption process happened in a shaking incubator at 21 °C and 250 rpm. The kinetics were determined by measuring the phosphate concentrations at time intervals of 30 mins, 1, 3, 6 h, 1, 2, 3, 4, 7 days, and 1, 2, 3 months. The shaking speed (or stirring rate) affects the external transfer from the bulk solution to the adsorbent boundary layer but not the internal diffusion to the adsorbent pores [27,29,30]. Thus it is enough to use a shaking speed that overcomes external mass transfer resistance. The shaking speed used here was based on the range provided by other studies involving porous phosphate adsorbents [18,29,31].

2.3. Phosphate adsorption isotherm experiments

The different adsorbents of the aforementioned particle size ranges were added to 100 ml solutions with phosphate concentrations of 1, 5, 10, 15, 25, 50, 75 and 100 mg P/L. MOPS buffer of 20 mM concentrations was used to buffer the pH which was adjusted to 7.2. The adsorbent concentration was 2 g/L. The adsorption process happened in a shaking incubator at 21 °C and 2500 rpm. The adsorption process was continued till 7 days after which the phosphate concentrations were measured.

2.4. Analysis

Phosphate concentration was measured by ion chromatrography (Metrohm Compact IC Flex 930). All samples were filtered by 0.45 μm membrane before analysis. The types of iron oxide in GEH, FSP, and CFH were determined using Mössbauer spectroscopy. Transmission ^{57}Fe Mössbauer spectra were collected at different temperatures with conventional constant acceleration and sinusoidal velocity spectrometers using a ^{57}Co (Rh) source. Velocity calibration was carried out using an α-Fe foil. The Mössbauer spectra were fitted using the Mosswin 4.0 program. The type of aluminium oxide in the adsorbent DD6 was measured by X-Ray Diffraction (XRD). The XRD measurements were carried out using a PANalytical X'Pert pro X-ray diffractometer mounted in the Bragg-Brentano configuration with a Cu anode (0.4 mm × 12 mm line focus, 45 kV, 40 mA). For determining the surface area of the adsorbents, nitrogen adsorption and desorption cycles were carried out using Micromeritics TriStar 3000. The data from the nitrogen adsorption-desorption profiles were fitted with models included in the analysis software to obtain the pore area from Non Local Density Functional Theory (NLDFT).

2.5. Data fitting and error analysis

All the adsorption experiments were run as duplicates and the average value was reported with standard deviation. For adsorption isotherms and pseudo second order kinetic models, model parameters were fitted with non-linear regression using Microsoft Excel's solver

program. The standard deviation of the parameter estimates ($\hat{\theta}$) were calculated using the covariance matrix, which is expressed as follows:

$$Cov(\hat{\theta}) = \frac{SSE(\hat{\theta})}{n-p}(X(\hat{\theta})^T X(\hat{\theta}))^{-1}$$

Where, n denotes the number of samples, p denotes the number of parameters, SSE ($\hat{\theta}$) denotes the sum of squared error between the experimental data and fitted model output, X($\hat{\theta}$) denotes the sensitivity matrix. The sensitivity matrix is calculated by analyzing the sensitivity of each parameters separately by ± 10% of their optimum value and quantifying the change in model output. The standard deviation of the parameter estimates are calculated by taking square root of the diagonal of the covariance matrix.

The Root Mean Square Error (RMSE) is used as measure of goodness of fit and is calculated as follows:

RMSE $\hat{\theta} = \sqrt{\frac{SSE(\hat{\theta})}{n-p}}$ Where, SSE ($\hat{\theta}$), n and p denote the same parameters as used in the covariance matrix.

Non-linear regression was used for the isotherm and kinetic models to avoid inaccuracies that occur due to linearization of such models [32,33]. While the coefficient of determination (R^2) can be used as a measure for the goodness of fit of linear models, they are not suitable for non-linear regression [34]. Hence, in this case, the RMSE, which is the standard deviation of residuals (difference between observed and fitted value) is used as a goodness of fit, with a lower RMSE value indicating a better fit. Moreover, the covariance matrix indicates the uncertainty in the parameter estimates, and thus is also indicative of the nature of the fit [35].

3. Results and discussion

3.1. Adsorbent characteristics

Table 1 shows the different characteristics of the adsorbents used. The type of metal oxide for iron based adsorbents was determined using Mössbauer spectroscopy (Mössbauer parameters shown in Table S2 in supporting information). The type of metal oxide for the aluminium based adsorbent DD6 was determined using XRD (Fig. S1 in supporting information shows the spectrogram).

As can be seen from Table 1, FSP and GEH predominantly comprised of ferrihydrite, although GEH had a small fraction of hematite. For CFH, the hyperfine fields could not be exactly assigned to a specific iron oxide and hence it could be a combination of iron oxides that include lepidocrocite as well as goethite. The XRD spectra of DD6 included peaks that corresponded to aluminium oxide as well as aluminum oxide hydroxide. The result shows that most of the adsorbents had a mixture of metal oxide types. This would lead to having heterogeneous sites for adsorption.

The total pore area was determined using the Non-Linear Density Functional Theory (NLDFT) model, incorporated within the software of the Micrometric nitrogen adsorption analyzer. The International Union of Pure and Applied Chemistry (IUPAC) classifies porous materials into 3 categories based on the pore diameters; namely, micropores (< 2 nm), mesopores (2–50 nm) and macropores (> 50 nm) [36,37]. Gas adsorption and desorption profiles can be fit with different models (inbuilt within the Micrometric software) to obtain information like the specific surface area, pore volume and pore size distribution [38]. While meso and macropores can be described by the classic/macroscopical models like BJH (Barret-Joyner-Halenda), the accurate description of micropores requires more modern models like NLDFT [39,40]. The mechanism of pore filling constitutes the main difference between these models. BJH model assumes that pore filling via pore condensation constitutes well defined interfaces in the pores. While this works for macropores and to the larger mesopores, the adsorptive potential between adsorbate and adsorbent plays a major influence in the condensation and evaporation from smaller mesopores and micropores [40]. The NLDFT model takes into account the differences in thermodynamic properties of a bulk fluid vs a fluid confined in pores [41]. Thus it is able to give a more accurate description of the micro and mesopores.

Table 1
Adsorbent characteristics.

Adsorbent	Type and proportion of constituent metal oxide(s)	Total pore area (m^2/g)[a]
GEH	Hematite – 11% Ferrihydrite – 89%	244
FSP	Ferrihydrite – 100%	179
CFH	Goethite/Hematite – 43% Ferrihydrite/Lepidocrocite – 57%	119
DD6	Aluminium oxide hydroxide – 34% Aluminium oxide – 66%	235

[a] The total pore area shown here is for the adsorbents of size 1–1.25 mm. However, the area of the adsorbents showed little change (a maximum change of < 5%) when the particle sizes were reduced (Table S1 in supporting information).

To get a complete picture of micro, meso and macropores, the adsorbents used were characterized using both the NLDFT and the BJH model (Fig. S2 in supporting information). The pore size distribution (PSD) of the adsorbents as determined by the NLDFT method is shown in Fig. 1. Henceforth, the term surface area actually implies the pore area.

As seen in Fig. 1, the adsorbents had very different PSD. Fig. 1 (a and b) show that the GEH and CFH had pores smaller than 10 nm. FSP and DD6 on the other hand had a significant fraction of pore volume resulting from pores bigger than 10 nm. Fig. 1 (c and d) show the area resulting from the corresponding pores in the adsorbent. This shows that GEH had significant pore area resulting from micropores as well as mesopores smaller than 10 nm, whereas CFH had a majority of pore area from the micropores. FSP and DD6 had pore area resulting from pores greater than 10 nm as well. Fig. 2 shows the relative fraction of micropore area, and mesopore areas that are between 2 and 10 nm and between 10 and 50 nm.

Fig. 2 shows that even though the pore volume resulting from micropores is lower than that from the mesopores for all adsorbents, the pore area of micropores has a significantly higher fraction. This was to be expected since smaller pores will have the highest area to volume ratio. Fig. 2 also shows that FSP has the highest amount of surface area resulting from pores bigger than 10 nm, followed by DD6. CFH and GEH have little to no surface area resulting from such pores. The area contributed by macropores was also negligible (Fig. S2 in supporting information). Since adsorption is a surface phenomenon depending on the area, very little phosphate adsorption will happen in macropores compared to micropores and mesopores. Nevertheless, macropores can still play a role by allowing faster diffusion of phosphate [42].

3.2. Adsorption kinetics for varying particle sizes and correlation with the PSD

The adsorption kinetics were done with varying particle sizes to understand how phosphate diffusion through the pores is affected with varying path lengths for diffusion. All the adsorbents were grinded between 3 particle size ranges: 1–1.25 mm, 0.4–0.5 mm, and 0–0.1 mm, henceforth called large, medium and small, respectively. Fig. 3 shows the adsorption kinetics for the different particle sizes of all adsorbents.

As seen in Fig. 3, the small particles of all adsorbents reached equilibrium by 7 days. For FSP and DD6, the large particles also almost reached equilibrium in 7 days. However, this was not the case for the large particles of GEH and CFH. To find out the time required to reach equilibrium for these particles, the adsorption kinetic experiments were prolonged. It was found that it took between 60 and 90 days for the large particles of GEH and CFH to reach equilibrium (see Fig. 4). This is

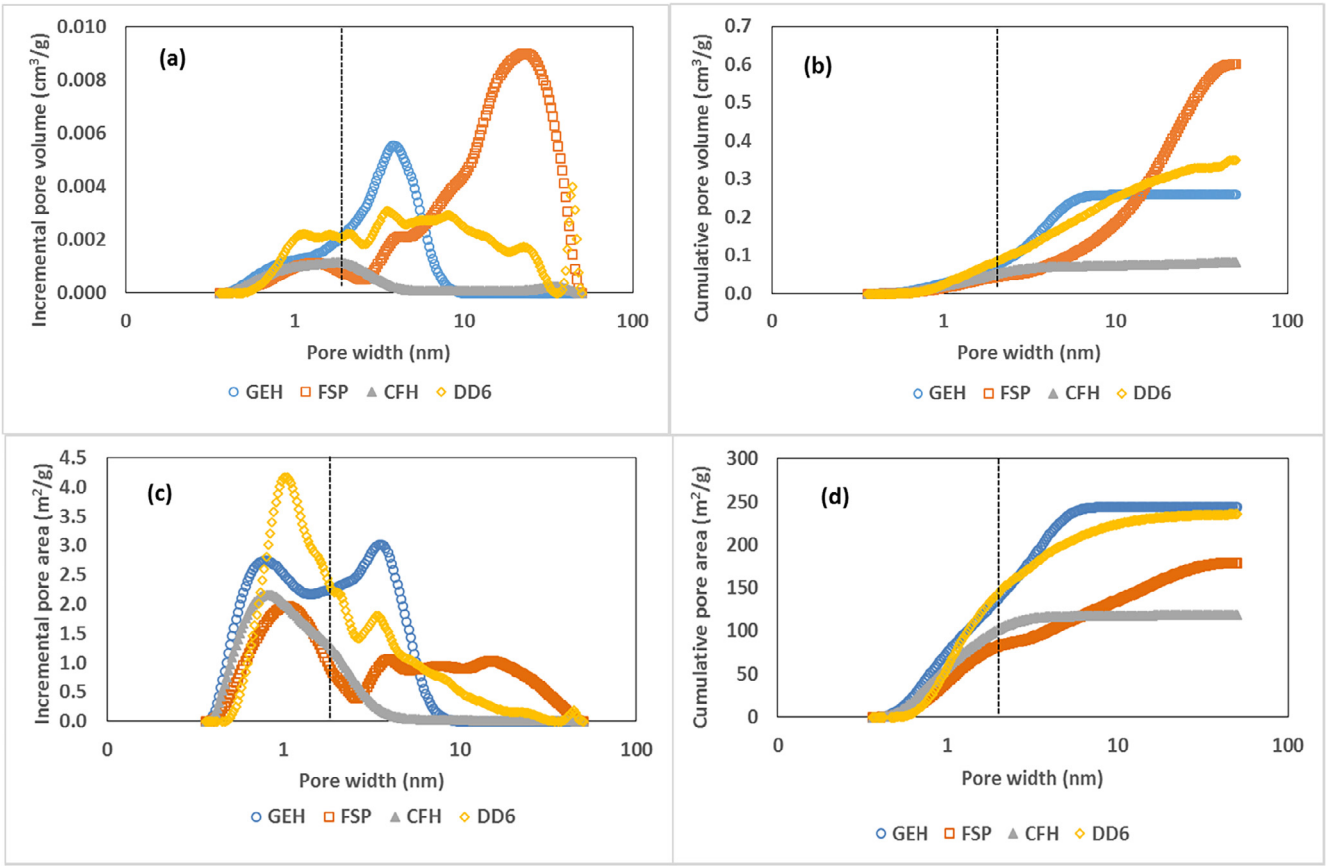

Fig. 1. (a) Incremental and (b) Cumulative pore volume of different adsorbents as determined by the NLDFT method. (c) Incremental and (d) Cumulative pore area for the corresponding adsorbents. The dashed lines within the plots show the cut off (2 nm) between micro and mesopores.

a significantly longer time than reported in most phosphate adsorption studies and shows that these adsorbents show severe diffusion limitation. As will be elaborated in the following sections, this is related to the PSD of these adsorbents.

To correlate these differences with the pore size distribution, the adsorption kinetics needed to be modelled. A pseudo second order kinetic model was chosen due to its basic nature and it has been commonly used for fitting phosphate adsorption kinetics [43–45]. It is described by the following expression:

$$q_t = \frac{(kq_e^2 t)}{(1 + (kq_e t))}$$

where, q_t is the adsorption capacity at time t, k is the adsorption rate constant (g/mg min), q_e is the adsorption capacity at equilibrium.

The parameters estimated from the pseudo second order kinetic model are shown in Table 2. The rate constant obtained from the pseudo second order model for different adsorbents was plotted as a function of the adsorbent particle size (Fig. 5).

As can be seen from Table 2 and Fig. 5, the rate constants for the small particle size of all adsorbents were in the same order of magnitude. However, as the particle size increased (> 0.4 mm) the rate constants for the different adsorbents varied as much as by an order of magnitude. For the large adsorbent particles, FSP and DD6 had rate constants that were higher by one order of magnitude compared to GEH and CFH. This implied the adsorption rate was higher for the large particles of FSP and DD6 compared to GEH and CFH, which can be seen from Fig. 3.

A ratio of the rate constant of the small (K_{Small}) to the large adsorbent (K_{Large}) can be used as an indication of the extent of diffusion limitation in this case. If this ratio of K_{Small}/K_{Large} is lower, this implies the adsorption kinetics is less effected by varying the particle size. To correlate this effect with the PSD, the ratio of the rate constant of small to the large adsorbent particles (K_{Small}/K_{Large}) was plotted against the pore area resulting from micropores (< 2 nm), pores between 2 and 10 nm, and pores greater than 10 nm, as shown in Fig. 6.

As can be seen from Fig. 6, GEH and CFH had a significantly higher K_{Small}/K_{Large} value than FSP and DD6, which correlates with the observation in Fig. 3 regarding the adsorption kinetics. Also, Fig. 6 (a and b) shows that no clear correlation could be made between the K_{Small}/K_{Large} values of the different adsorbents and the microporous area and the area resulting from pores between 2 and 10 nm. For instance, GEH had a higher microporous area as well as area from pores between 2 and 10 nm, but still showed a higher variation in the adsorption kinetic constants. This implies that the adsorption kinetics are not dominated by the pores in the size ranges that are smaller than 10 nm.

However, a correlation could be observed between K_{Small}/K_{Large} values of the adsorbents and the area resulting from pores bigger than 10 nm (Fig. 6 c). The K_{Small}/K_{Large} values varied inversely with the area resulting from pores bigger than 10 nm. In practice the rate constant for a smaller particle will always be higher than the rate constant for a larger particle of the corresponding adsorbent. Thus K_{Small}/K_{Large} value will always be higher than 1. The plot in Fig. 6 c is in line with this expected asymptote at value 1 as the area from pores bigger than 10 nm keeps increasing. This correlation was also observed with the pore volume from such mesopores (Fig. S3 in supporting information). This shows that having pores bigger than 10 nm is crucial for improving the phosphate adsorption kinetics of granular porous metal oxides.

3.3. Adsorption isotherms for varying particle sizes

Adsorption isotherms are an important tool that provide phosphate adsorption capacities over a wide range of phosphate concentration.

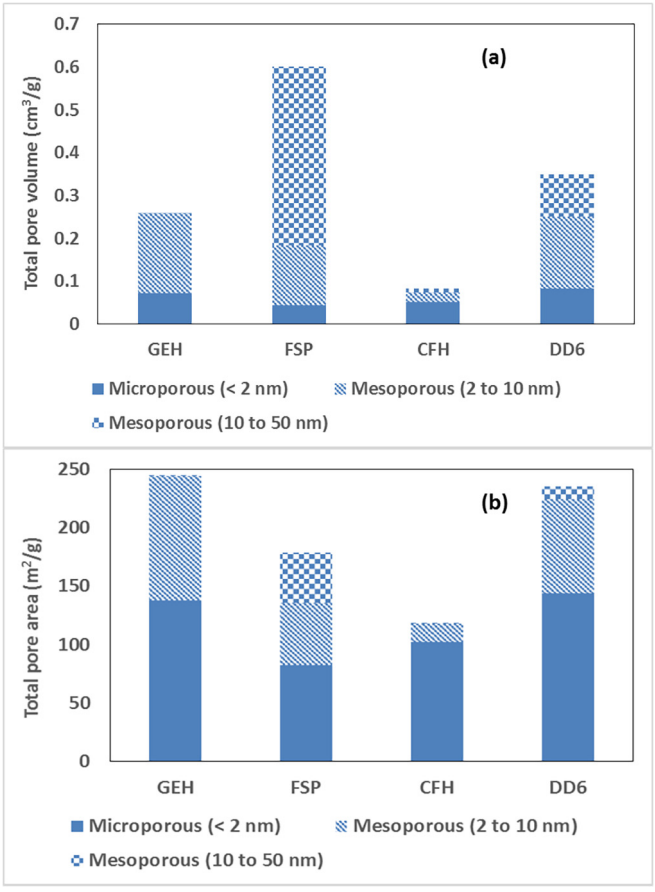

Fig. 2. Relative fractions for microporous, mesoporous (a) pore volume and (b) pore area in the different adsorbents. The mesoporous fraction is split further at the cut-off of 10 nm.

The adsorption kinetics experiment showed that the small sized particles of all adsorbents reached equilibrium by 7 days. Thus the adsorption isotherms were run for 7 days for all the particle sizes to see the effect of diffusion limitation over different phosphate concentrations. Fig. 7 shows the adsorption isotherms of the different adsorbents of the varying particle sizes after allowing adsorption for 7 days.

Fig. 7 shows that for the small particles of all adsorbents, similar experimental adsorption capacities around 25 mg P/g were observed at final concentrations of 40–50 mg P/L. Morevoer the adsorption isotherms for the different adsorbents correlated with the observations in the adsorption kinetic studies. That is, varying particle sizes of FSP and DD6 showed similar adsorption profiles. This agrees with the fact that these adsorbents reached equilibrium by 7 days for all particle sizes. GEH and CFH on the other hand showed differences in the adsorption profiles between the varying particle sizes. This agrees with the fact that the medium and larger sized granules of such adsorbents need a much longer time for reaching equilibrium. Modelling the equilibrium adsorption data allows the prediction of adsorption capacities at different phosphate concentrations. As seen earlier, the small particles had reached equilibrium by 7 days for all the adsorbents. Hence the isotherms from the small sized adsorbent particles were chosen to be modelled.

The Langmuir and Freundlich adsorption isotherm models are commonly used for describing phosphate adsorption [11,13,46,47].

The Langmuir expression is:

$$q_e = \frac{q_m K_L C_e}{(1 + K_L C_e)}$$

Where

q_m = Maximum adsorption capacity (mg P/g),
q_e = Adsorption capacity at equilibrium (mg P/g),
C_e = Concentration at equilibrium (mg P/L),
K_L = Langmuir isotherm constant (L/mg P).

The Freundlich expression is:

$$q_e = K_F C_e^n$$

Where

q_e = Adsorption capacity at equilibrium (mg P/g),
C_e = Concentration at equilibrium (mg P/L),
n = Adsorption intensity (heterogeneity factor),
K_F = Freundlich isotherm constant ((mg P/g)/(mg P/L)^n)

Since phosphate adsorption onto metal oxides happens by ligand exchange/chemisorption (thus excluding multilayer adsorption), the main difference between the assumptions of Langmuir and Freundlich models in this case lies in the nature of the active sites for adsorption. Langmuir model assumes homogenous active sites, whereas Freundlich model assumes heterogenous active sites [48–50]. Thus the Freundlich model implies that phosphate will bind on the adsorbent at active sites having different heat of adsorption and affinities [50]. Table 3 shows the fitted values of the parameters from these models and the corresponding Root Mean Square Error (RMSE).

As can be seen from the RMSE values in Table 3, the Langmuir model gave a better fit than the Freundlich model for all adsorbents except FSP. However, it can be seen from Fig. 7 that neither adsorption model fitted the experimental data perfectly over the complete range of phosphate concentrations. The Langmuir model gave a better fit over the lower concentration ranges and the Freundlich model gave a better fit over the higher concentration ranges. Since most of the adsorbents comprised of multiple phases/types of metal oxides, it could be that at lower phosphate concentrations one of the metal oxides were preferred for phosphate adsorption thus resembling the Langmuir fit better. At higher phosphate concentration, the fraction of active sites occupied by other metal oxide phases might become important as well. This would lead to a heterogenous nature of adsorption and thereby resemble the Freundlich fit better at such concentrations.

Another explanation could be the formation of surface precipitates at higher phosphate concentration [51]. Even though the adsorbents were washed with MilliQ (deionized) water before the adsorption experiments, during the course of 7 days, some soluble components of the adsorbent (e.g. iron and aluminium) inside the pores might result in surface precipitation with phosphate. Surface precipitation will follow a reaction mechanism that will be different than adsorption [51]. This will show an increased removal and hence might lead to a higher apparent adsorption capacity than the monolayer adsorption predicted by Langmuir model.

The adsorption isotherms can help get an estimate of the fraction of adsorbent surface area covered by phosphate at different equilibrium concentrations. The phosphate molecule has a diameter of about 0.48 nm [52], and assuming a monolayer, this approximately translates to a cross sectional area of 3.5 m^2/mg P. Table 4 shows the fractions of adsorbent surface area occupied at the maximum adsorption capacity and the adsorption capacity at an equilibrium phosphate concentration of 0.1 mg P/L ($q_{0.1}$) as estimated from the Langmuir equation. $q_{0.1}$ is relevant considering the need for achieving very low concentrations of phosphate via adsorption.

Table 4 shows that CFH had the highest fraction of adsorbent surface coverage for both q_m as well as $q_{0.1}$. In all other cases, less than 1/7th of the adsorbent surface area is occupied at $q_{0.1}$. This shows that only a small fraction of the adsorbent surface area is covered at equilibrium phosphate concentrations of 0.1 mg P/L. Another conclusion that can be drawn from this observation is regarding the contribution of micropores. CFH has about 85% of its surface area coming from

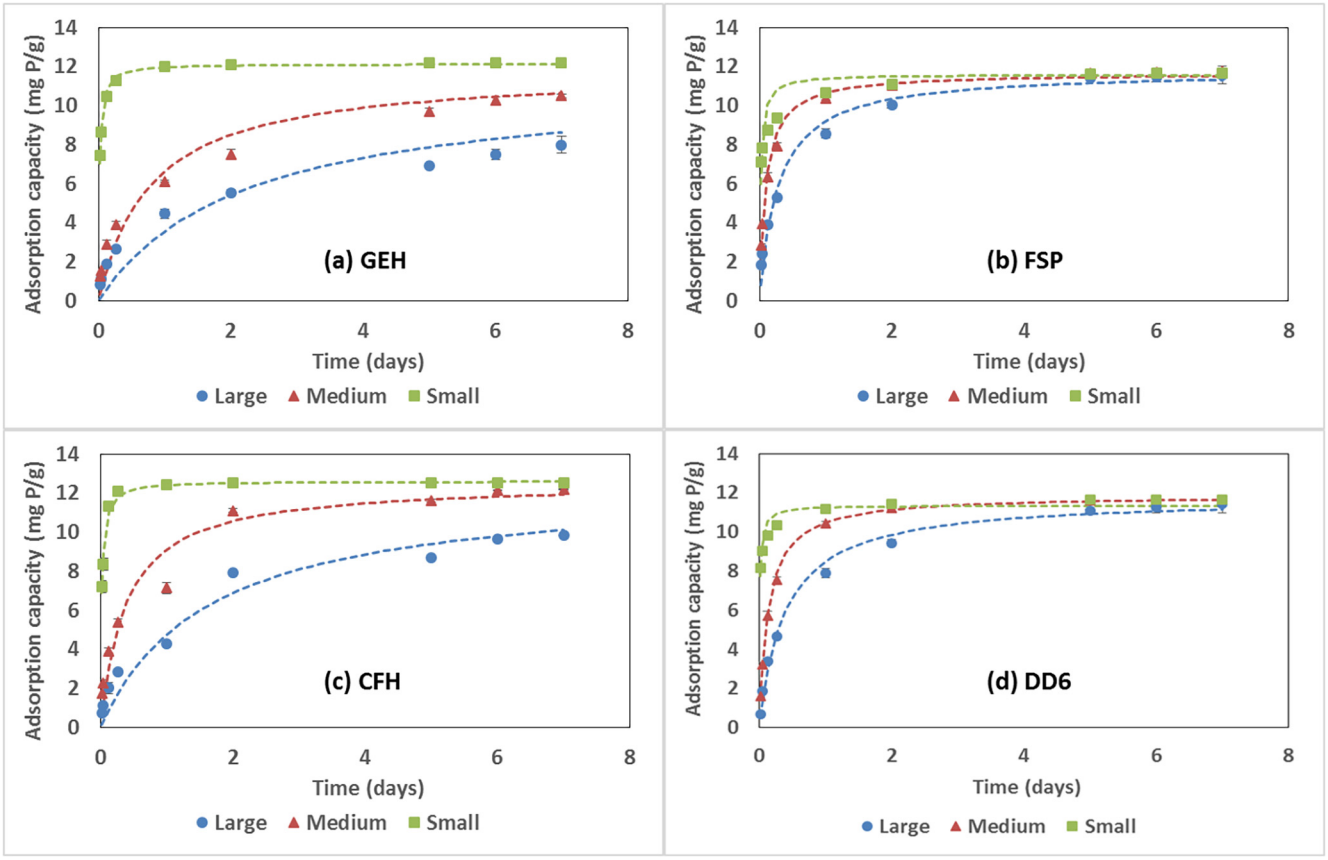

Fig. 3. Adsorption kinetics for different sizes of adsorbents (a) GEH (b) FSP (c) CFH (d) DD6. Dashed lines represent fit by the pseudo second order kinetics.

micropores (Fig. 2 b) and the occupancy by phosphate is between 34 and 78 % of the surface area of CFH. Thus it can be concluded that the micropores do contribute to phosphate adsorption.

3.4. Possible explanations for diffusion limitation

The severe diffusion limitation shown by larger adsorbent particles for GEH and CFH can be seen from the adsorption kinetics (Figs. 3 and 4). By modelling with the pseudo-second order kinetic model, it could be shown that pores bigger than 10 nm are essential for allowing fast transport of phosphate through the adsorbent. While the pseudo second order kinetic model was useful in correlating the adsorption kinetics to the PSD, it is an empirical model and does not give an insight into the mechanism of phosphate adsorption kinetics [53]. The adsorption kinetics were thus also modelled by a pore diffusion model (PDM), which is a more mechanistic model considering Fick's laws of diffusion for estimating the effective pore diffusivity and external film mass transfer coefficient [22]. However, this model gave a poorer fit than the pseudo second order model and hence was not considered further. Amongst the major limitations from the current PDM is the fact that it considers the adsorbent particle size to be all the same. In practice the adsorbents will have a particle size distribution. Moreover it takes into account the adsorbent particle porosity, but it does not differentiate between the porosity contributed by micro, meso or macropores. Also, adsorption could be happening via a combination of pore and surface diffusion [54], in which case pore diffusion alone will not be able to give a

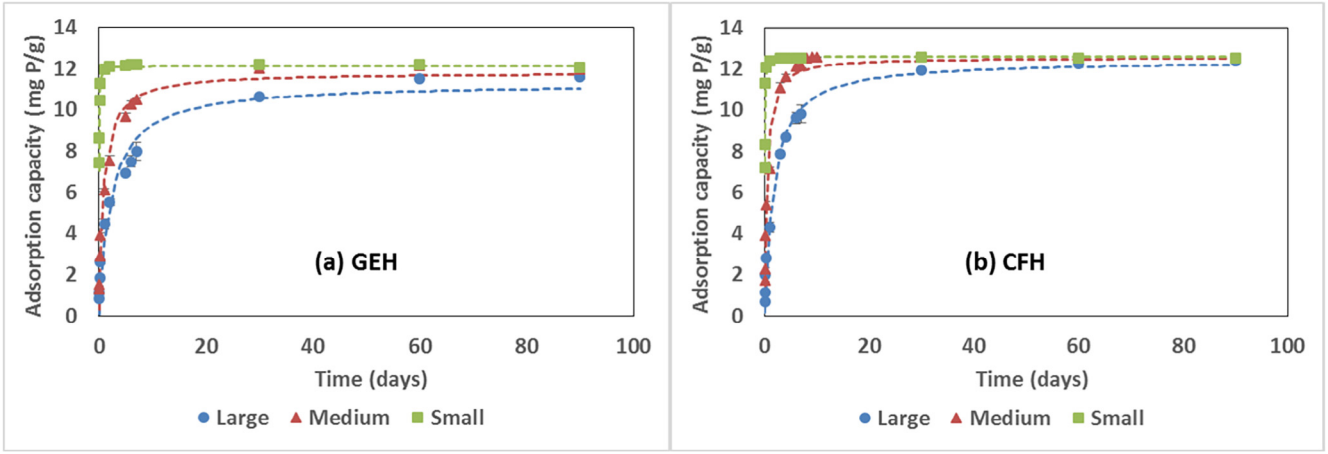

Fig. 4. Adsorption kinetics performed upto 90 days as a function of different particle sizes for (a) GEH (b) CFH.

Table 2
Pseudo-second order kinetic model fitted parameters.

Adsorbent/Particle Size	Large	Medium	Small
GEH	q_e(mg P/g) = 11.3 ± 2.1 k (g/mg min) = $2.8 \times 10^{-5} \pm 2.6 \times 10^{-6}$ RMSE = 0.9	q_e(mg P/g) = 11.8 ± 0.9 k (g/mg min) = $7.5 \times 10^{-5} \pm 9.6 \times 10^{-6}$ RMSE = 0.8	q_e(mg P/g) = 12.1 ± 0.1 k (g/mg min) = $3.8 \times 10^{-3} \pm 1.8 \times 10^{-4}$ RMSE = 0.2
FSP	q_e(mg P/g) = 11.8 ± 0.4 k (g/mg min) = $2.1 \times 10^{-4} \pm 9.5 \times 10^{-6}$ RMSE = 0.6	q_e(mg P/g) = 11.7 ± 0.3 k (g/mg min) = $6.2 \times 10^{-4} \pm 5 \times 10^{-5}$ RMSE = 0.4	q_e(mg P/g) = 11.6 ± 0.4 k (g/mg min) = $3.1 \times 10^{-3} \pm 2.1 \times 10^{-4}$ RMSE = 0.9
CFH	q_e(mg P/g) = 12.4 ± 1.2 k (g/mg min) = $3.4 \times 10^{-5} \pm 1.7 \times 10^{-6}$ RMSE = 0.6	q_e(mg P/g) = 12.6 ± 0.5 k (g/mg min) = $1.5 \times 10^{-4} \pm 2.1 \times 10^{-5}$ RMSE = 0.8	q_e(mg P/g) = 12.6 ± 0.1 k (g/mg min) = $3.1 \times 10^{-3} \pm 4.7 \times 10^{-4}$ RMSE = 0.2
DD6	q_e(mg P/g) = 11.8 ± 0.5 k (g/mg min) = $1.5 \times 10^{-4} \pm 3.5 \times 10^{-6}$ RMSE = 0.4	q_e(mg P/g) = 11.9 ± 0.2 k (g/mg min) = $4.4 \times 10^{-4} \pm 3.1 \times 10^{-5}$ RMSE = 0.2	q_e(mg P/g) = 11.3 ± 0.2 k (g/mg min) = $6.3 \times 10^{-3} \pm 2.9 \times 10^{-4}$ RMSE = 0.4

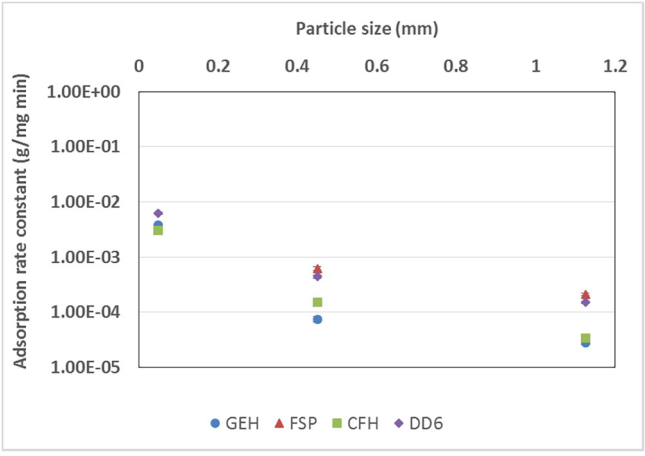

Fig. 5. Pseudo second order rate constants as a function of particle size of different adsorbents. Particle sizes were considered as 0.05 mm, 0.45 mm, 1.125 mm since they represented the average values between the particle size ranges of 0–0.1, 0.4–0.5 and 1–1.25 mm. The adsorption rate constant is presented on a log scale.

sufficient description.

Moreover, it is not just the PSD, but also the 3 dimensional arrangement of the pores that would play a key role in diffusion of an adsorbate ion through the adsorbent [55]. Techniques such as focused ion beam scanning electron microscopy (FIBSEM) can be used to obtain 3D information of porous structures [56]. A phosphate molecule has a size of 0.48 nm and once they are adsorbed in micropores (pore width < 2 nm), they could hinder the subsequent transport of other phosphate molecules through the micropores. This will also depend on the arrangement of micropores, i.e. if they are highly branched or exist as long isolated cylinders. In the latter case, the adsorbed phosphate molecule has to diffuse along the surface before a subsequent phosphate molecule can travel through the pore and adsorb. The diffusion could also be affected by the formation of hydration shells [57]. Such factors would lead to hindered diffusion through small pores which would slow down the rate of phosphate adsorption [58]. More detailed models considering all these parameters can give a better insight into the adsorption mechanism. The downside with such models could be the complexity involved in solving such models accurately to estimate the mass transfer coefficients or adsorption rate constants. It would be practical to study such models in conjunction with column studies and model the kinetic data based on realistic hydraulic retention times.

4. Conclusion

This study determined the effect of pore size distribution (PSD) on

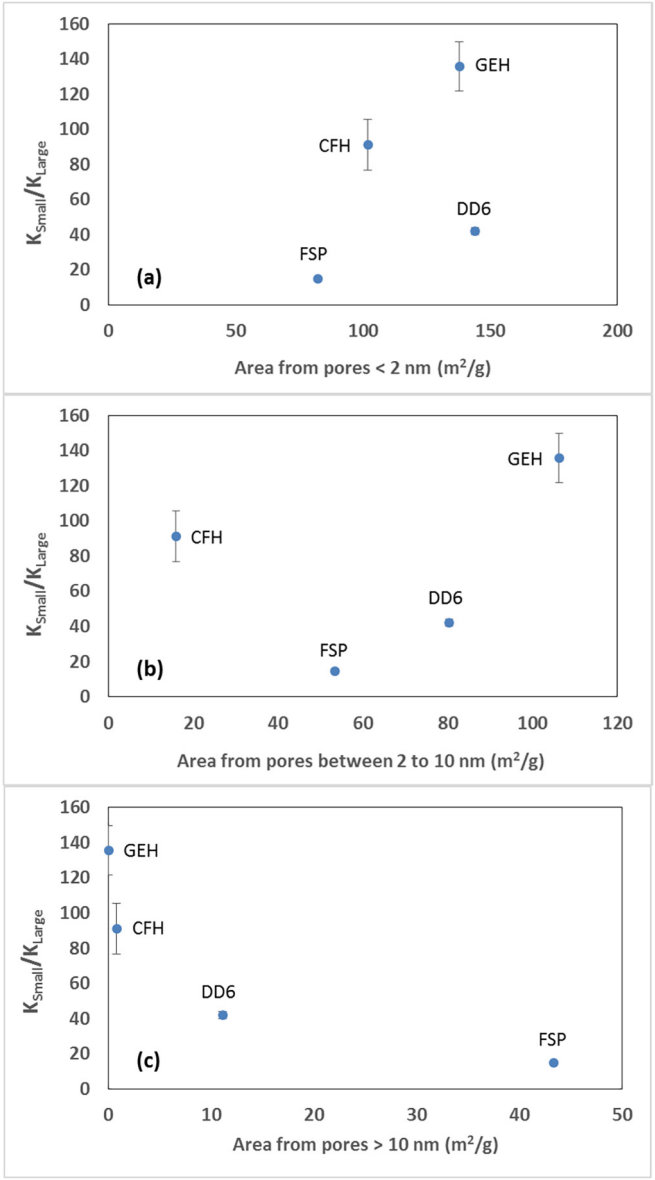

Fig. 6. Ratio of rate constants from pseudo second order kinetic model of small (0–0.1 mm) to large particles (1–1.25 mm) for the different adsorbents as a function of (a) Area by pores less than 2 nm (b) Area by pores between 2 and 10 nm (c) Area by pores greater than 10 nm.

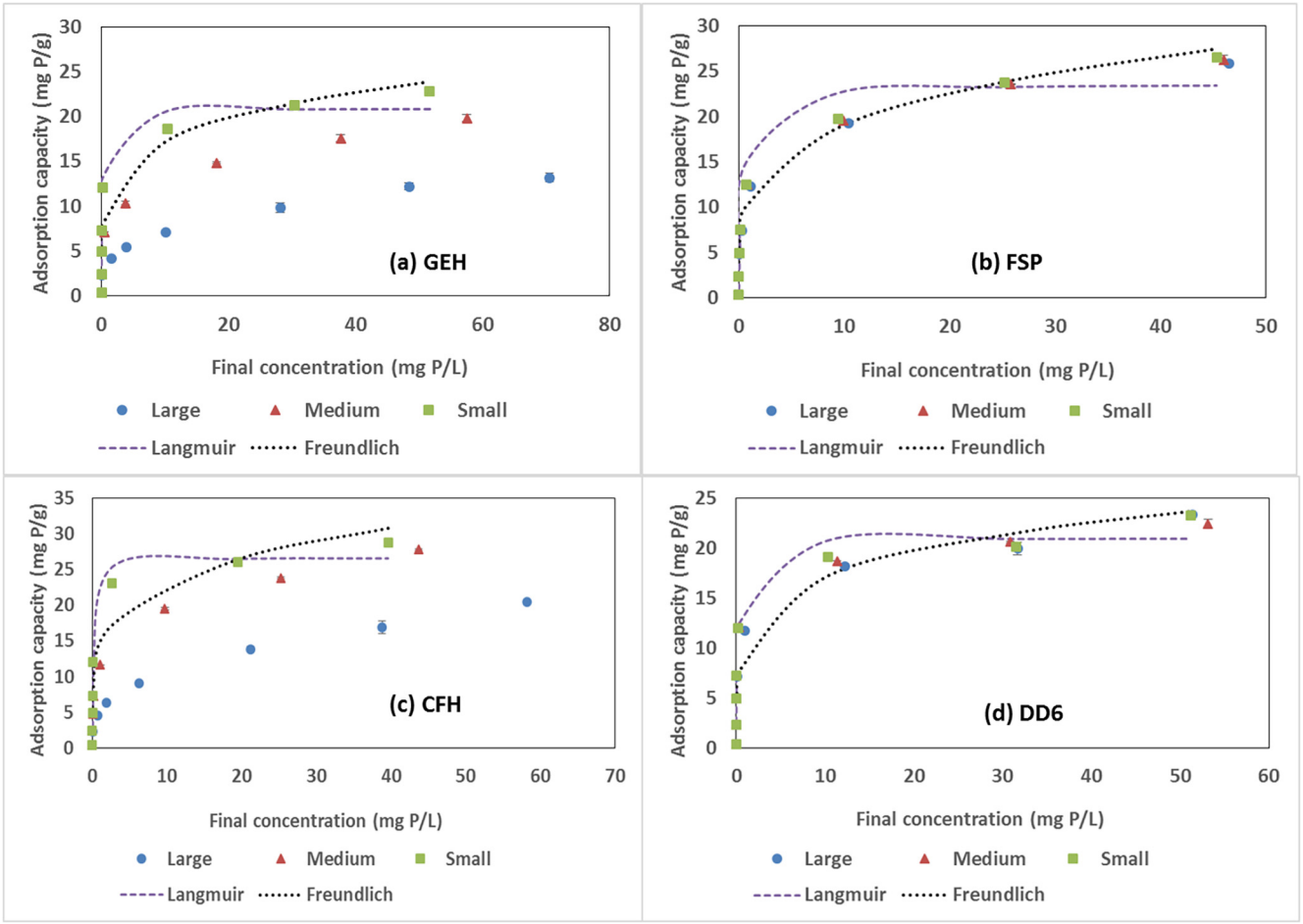

Fig. 7. Adsorption capacities as a function of final concentration after 7 days for different sizes of adsorbents (a) GEH (b) FSP (c) CFH (d) DD6. The dashed plot shows the fits with Langmuir and Freundlich models of the small adsorbent particles.

Table 3
Isotherm parameters for small particles of different adsorbents.

Adsorbent/ Isotherm model	Freundlich	Langmuir
GEH	K_F ((mg P/g)/(mg P/L)^n) = 10.8 ± 3.7 n = 0.2 ± 0.1 RMSE = 2.8	K_L (L/mg P) = 7.6 ± 1 q_m (mg P/g) = 20.9 ± 1.8 RMSE = 1.7
FSP	K_F ((mg P/g)/(mg P/L)^n) = 10.9 ± 1.8 n = 0.2 ± 0.05 RMSE = 2	K_L (L/mg P) = 2.3 ± 1.7 q_m (mg P/g) = 23.6 ± 1 RMSE = 2.7
CFH	K_F ((mg P/g)/(mg P/L)^n) = 13.9 ± 4.2 n = 0.2 ± 0.09 RMSE = 4	K_L (L/mg P) = 7.6 ± 1.1 q_m (mg P/g) = 26.6 ± 1.5 RMSE = 1.9
DD6	K_F ((mg P/g)/(mg P/L)^n) = 10.8 ± 4.2 n = 0.2 ± 0.1 RMSE = 2.9	K_L (L/mg P) = 8.4 ± 0.9 q_m (mg P/g) = 20.9 ± 1.7 RMSE = 1.6

phosphate adsorption. Varying the adsorbent particle size allowed the difference in adsorption to be correlated directly with the diffusion into the pores. Adsorption kinetic experiments showed that equilibrium was reached within 7 days for all particle sizes of FSP and DD6, whereas the medium (0.4–0.5 mm) and large (1–1.25 mm) particles of GEH and CFH required 60–90 days to reach equilibrium. The adsorption kinetics were fitted by a pseudo second order model and the ratio of rate constants of the large to small particles, i.e. K_{Small}/K_{Large} was used as an indication to understand the diffusion limitation. This ratio was correlated with the adsorbent PSD to show that pore sizes greater than 10 nm are required for good adsorption kinetics.

Table 4
Fraction of adsorbent surface area occupied at maximum adsorption capacity and adsorption capacity at equilibrium concentration of 0.1 mg P/L, i.e. $q_{0.1}$. The fraction of surface area occupied is calculated assuming monolayer coverage, and the $q_{0.1}$ is calculated using the Langmuir equation.

Adsorbents	q_m (mg P/g)	Fraction of surface area occupied at q_m (%)	$q_{0.1}$ (mg P/g)	Fraction of surface area occupied at $q_{0.1}$ (%)
GEH	20.9	30	9	13
FSP	23.6	46	4.4	9
CFH	26.6	78	11.5	34
DD6	20.9	31	9.5	14

The insights from this study will help to design granular porous phosphate adsorbents with an appropriate PSD. This is necessary to obtain high phosphate adsorption capacities in relatively short contact times. Future studies should include modelling the adsorption kinetics in a column mode at more realistic contact times. More holistic studies on the pore structure of adsorbent must include the 3 dimensional arrangement of the pores apart from the PSD.

Acknowledgements

This work was performed in the TTIW-cooperation framework of Wetsus, European Centre Of Excellence For Sustainable Water Technology (www.wetsus.nl). Wetsus is funded by the Dutch Ministry of Economic Affairs, the European Union Regional Development Fund, the Province of Fryslân, the City of Leeuwarden and the EZ/Kompas program of the "Samenwerkingsverband Noord-Nederland". We thank the participants of the research theme "Phosphate Recovery" for their financial support and helpful discussions.

Appendix A. Supplementary data

Supplementary data to this article can be found online at https://doi.org/10.1016/j.cej.2018.09.202.

References

[1] K. Ashley, D. Cordell, D. Mavinic, A brief history of phosphorus: from the philosopher's stone to nutrient recovery and reuse, Chemosphere 84 (2011) 737–746.
[2] D. Cordell, J.-O. Drangert, S. White. The Story of Phosphorus: Global Food Security and Food for Thought, 2009.
[3] L. Carvalho, C. McDonald, C. Hoyos, U. Mischke, G. Phillips, G. Borics, S. Poikane, B. Skjelbred, L. Solheim Anne, J. Wichelen, C. Cardoso Ana, Sustaining recreational quality of European lakes: minimizing the health risks from algal blooms through phosphorus control, J. Appl. Ecol. 50 (2013) 315–323.
[4] C.J. Richardson, R.S. King, S.S. Qian, P. Vaithiyanathan, R.G. Qualls, C.A. Stow, Estimating ecological thresholds for phosphorus in the everglades, Environ. Sci. Technol. 41 (2007) 8084–8091.
[5] M.J. Maccoux, A. Dove, S.M. Backus, D.M. Dolan, Total and soluble reactive phosphorus loadings to Lake Erie: a detailed accounting by year, basin, country, and tributary, J. Great Lakes Res. 42 (2016) 1151–1165.
[6] M. Mekonnen Mesfin, Y. Hoekstra Arjen, Global anthropogenic phosphorus loads to freshwater and associated grey water footprints and water pollution levels: a high-resolution global study, Water Resour. Res. 54 (2017) 345–358.
[7] P. Hoagland, D.M. Anderson, Y. Kaoru, A.W. White, The economic effects of harmful algal blooms in the United States: estimates, assessment issues, and information needs, Estuaries 25 (2002) 819–837.
[8] V.H. Smith, G.D. Tilman, J.C. Nekola, Eutrophication: impacts of excess nutrient inputs on freshwater, marine, and terrestrial ecosystems, Environ. Pollut. 100 (1999) 179–196.
[9] J.N. Pretty, C.F. Mason, D.B. Nedwell, R.E. Hine, S. Leaf, R. Dils, Environmental costs of freshwater eutrophication in england and wales, Environ. Sci. Technol. 37 (2003) 201–208.
[10] L.M. Blaney, S. Cinar, A.K. SenGupta, Hybrid anion exchanger for trace phosphate removal from water and wastewater, Water Res. 41 (2007) 1603–1613.
[11] A. Genz, A. Kornmüller, M. Jekel, Advanced phosphorus removal from membrane filtrates by adsorption on activated aluminium oxide and granulated ferric hydroxide, Water Res. 38 (2004) 3523–3530.
[12] I. Midorikawa, H. Aoki, A. Omori, T. Shimizu, Y. Kawaguchi, K. Kassai, T. Murakami, Recovery of high purity phosphorus from municipal wastewater secondary effluent by a high-speed adsorbent, Water Sci. Technol. 58 (2008) 1601.
[13] E.A. Deliyanni, E.N. Peleka, N.K. Lazaridis, Comparative study of phosphates removal from aqueous solutions by nanocrystalline akaganéite and hybrid surfactant-akaganéite, Sep. Purif. Technol. 52 (2007) 478–486.
[14] W. Huang, X. Yu, J. Tang, Y. Zhu, Y. Zhang, D. Li, Enhanced adsorption of phosphate by flower-like mesoporous silica spheres loaded with lanthanum, Microporous Mesoporous Mater. 217 (2015) 225–232.
[15] Y. Su, H. Cui, Q. Li, S. Gao, J.K. Shang, Strong adsorption of phosphate by amorphous zirconium oxide nanoparticles, Water Res. 47 (2013) 5018–5026.
[16] S. Recillas, A. Garcia, E. Gonzalez, E. Casals, V. Puntes, A. Sanchez, X. Font, Preliminary study of phosphate adsorption onto cerium oxide nanoparticles for use in water purification; nanoparticles synthesis and characterization, Water Sci. Technol. 66 (2012) 503–509.
[17] R.F.P.M. Moreira, S. Vandresen, D.B. Luiz, H.J. José, G.L. Puma, Adsorption of arsenate, phosphate and humic acids onto acicular goethite nanoparticles recovered from acid mine drainage, J. Environ. Chem. Eng. 5 (2017) 652–659.
[18] A. Zach-Maor, R. Semiat, H. Shemer, Synthesis, performance, and modeling of immobilized nano-sized magnetite layer for phosphate removal, J. Colloid Interface Sci. 357 (2011) 440–446.
[19] N.I. Chubar, V.A. Kanibolotskyy, V.V. Strelko, G.G. Gallios, V.F. Samanidou, T.O. Shaposhnikova, V.G. Milgrandt, I.Z. Zhuravlev, Adsorption of phosphate ions on novel inorganic ion exchangers, Colloids Surf., A 255 (2005) 55–63.
[20] P. Suresh Kumar, T. Prot, L. Korving, K.J. Keesman, I. Dugulan, M.C.M. van Loosdrecht, G.-J. Witkamp, Effect of pore size distribution on iron oxide coated granular activated carbons for phosphate adsorption – Importance of mesopores, Chem. Eng. J. 326 (2017) 231–239.
[21] J. Lalley, C. Han, G.R. Mohan, D.D. Dionysiou, T.F. Speth, J. Garland, M.N. Nadagouda, Phosphate removal using modified Bayoxide[registered sign] E33 adsorption media, Environ. Sci. Water Res. Technol. 1 (2015) 96–107.
[22] L. Boels, K.J. Keesman, G.J. Witkamp, Adsorption of phosphonate antiscalant from reverse osmosis membrane concentrate onto granular ferric hydroxide, Environ. Sci. Technol. 46 (2012) 9638–9645.
[23] V. Barrón, J. Torrent, Surface hydroxyl configuration of various crystal faces of hematite and goethite, J. Colloid Interface Sci. 177 (1996) 407–410.
[24] R. Chitrakar, S. Tezuka, A. Sonoda, K. Sakane, K. Ooi, T. Hirotsu, Phosphate adsorption on synthetic goethite and akaganeite, J. Colloid Interface Sci. 298 (2006) 602–608.
[25] R.M. Cornell, U. Schwertmann, Adsorption of Ions and Molecules. The Iron Oxides, Wiley-VCH Verlag GmbH & Co. KGaA, 2004, pp. 253–296.
[26] A. Karau, C. Benken, J. Thommes, M.R. Kula, The influence of particle size distribution and operating conditions on the adsorption performance in fluidized beds, Biotechnol. Bioeng. 55 (1997) 54–64.
[27] A. Liese, L. Hilterhaus, Evaluation of immobilized enzymes for industrial applications, Chem. Soc. Rev. 42 (2013) 6236–6249.
[28] Y. Mao, A. Ninh Pham, Y. Xin, T. David Waite, Effects of pH, floc age and organic compounds on the removal of phosphate by pre-polymerized hydrous ferric oxides, Sep. Purif. Technol. 91 (2012) 38–45.
[29] K. Urano, H. Tachikawa, Process development for removal and recovery of phosphorus from wastewater by a new adsorbent. II. Adsorption rates and breakthrough curves, Ind. Eng. Chem. Res. 30 (1991) 1897–1899.
[30] A. Corma, V. Fornés, R.M. Martín-Aranda, H. García, J. Primo, Zeolites as base catalysts: Condensation of aldehydes with derivatives of malonic esters, Applied Catalysis 59 (1990) 237–248.
[31] E.W. Shin, J.S. Han, M. Jang, S.-H. Min, J.K. Park, R.M. Rowell, Phosphate adsorption on aluminum-impregnated mesoporous silicates: surface structure and behavior of adsorbents, Environ. Sci. Technol. 38 (2004) 912–917.
[32] T.A. Osmari, R. Gallon, M. Schwaab, E. Barbosa-Coutinho, J.B. Severo, J.C. Pinto, Statistical analysis of linear and non-linear regression for the estimation of adsorption isotherm parameters, Adsorpt. Sci. Technol. 31 (2013) 433–458.
[33] B. Subramanyam, A. Das, Linearized and non-linearized isotherm models comparative study on adsorption of aqueous phenol solution in soil, Int. J. Environ. Sci. Technol. 6 (2009) 633–640.
[34] A.-N. Spiess, N. Neumeyer, An evaluation of R(2)as an inadequate measure for nonlinear models in pharmacological and biochemical research: a Monte Carlo approach, BMC Pharmacol. 10 (2010) 6.
[35] K.J. Keesman, System identification: an introduction, Springer Science & Business Media, 2011.
[36] K.S. Sing, Reporting physisorption data for gas/solid systems with special reference to the determination of surface area and porosity (Recommendations 1984), Pure Appl. Chem. 57 (1985) 603–619.
[37] J. Rouquerol, D. Avnir, C. Fairbridge, D. Everett, J. Haynes, N. Pernicone, J. Ramsay, K. Sing, K. Unger, Recommendations for the characterization of porous solids, Pure Appl. Chem. 66 (1994) 1739–1758 (Technical Report).
[38] K. Sing, The use of nitrogen adsorption for the characterisation of porous materials, Colloids Surf., A 187–188 (2001) 3–9.
[39] E.P. Barrett, L.G. Joyner, P.P. Halenda, The determination of pore volume and area distributions in porous substances. I. Computations from nitrogen isotherms, J. Am. Chem. Soc. 73 (1951) 373–380.
[40] R.F. Cracknell, K.E. Gubbins, M. Maddox, D. Nicholson, Modeling fluid behavior in well-characterized porous materials, Acc. Chem. Res. 28 (1995) 281–288.
[41] M. Thommes, Physical adsorption characterization of ordered and amorphous mesoporous materials, Nanoporous Materials: Science and Engineering, Imperial College Press and Distributed by World Scientific Publishing Co., 2004, pp. 317–364.
[42] K.R. Végh, G.Y. Füleky, T. Varró, Phosphorus diffusion to barley (Hordeum vulgare) roots as influenced by moisture and phosphorus content of soils, in: M.L. van Beusichem (Ed.), Plant Nutrition — Physiology and Applications: Proceedings of the Eleventh International Plant Nutrition Colloquium, 30 July–4 August 1989, Wageningen, Springer Netherlands, Dordrecht, The Netherlands, 1990, pp. 147–151.
[43] A. Drenkova-Tuhtan, M. Schneider, M. Franzreb, C. Meyer, C. Gellermann, G. Sextl, K. Mandel, H. Steinmetz, Pilot-scale removal and recovery of dissolved phosphate from secondary wastewater effluents with reusable ZnFeZr adsorbent @ Fe3O4/SiO2 particles with magnetic harvesting, Water Res. 109 (2017) 77–87.
[44] K.-W. Jung, S. Lee, Y.J. Lee, Synthesis of novel magnesium ferrite (MgFe2O4)/biochar magnetic composites and its adsorption behavior for phosphate in aqueous solutions, Bioresour. Technol. 245 (2017) 751–759.
[45] J.-H. Park, J.J. Wang, S.-H. Kim, J.-S. Cho, S.-W. Kang, R.D. Delaune, D.-C. Seo, Phosphate removal in constructed wetland with rapid cooled basic oxygen furnace slag, Chem. Eng. J. 327 (2017) 713–724.
[46] X. Wang, F. Liu, W. Tan, W. Li, X. Feng, D. Sparks, Characteristics of phosphate adsorption-desorption onto ferrihydrite: comparison with well-crystalline Fe (Hydr) oxides, Soil Sci. 178 (2013) 1–11.
[47] G. Guzmán, E. Alcantara, V. Barrón, J. Torrent, Phytoavailability of phosphate adsorbed on ferrihydrite, hematite, and goethite, Plant Soil 159 (1994) 219–225.
[48] I. Langmuir, The adsorption of gases on plane surfaces of glass, mica and platinum, J. Am. Chem. Soc. 40 (1918) 1361–1403.
[49] H. Freundlich, Über die adsorption in lösungen, Z. Phys. Chem. 57 (1907) 385–470.
[50] K.Y. Foo, B.H. Hameed, Insights into the modeling of adsorption isotherm systems, Chem. Eng. J. 156 (2010) 2–10.
[51] L. Li, R. Stanforth, Distinguishing adsorption and surface precipitation of phosphate on goethite (α-FeOOH), J. Colloid Interface Sci. 230 (2000) 12–21.
[52] D.S. Tawfik, R.E. Viola, Arsenate replacing phosphate: alternative life chemistries and ion promiscuity, Biochemistry 50 (2011) 1128–1134.
[53] V. Russo, M. Trifuoggi, M. Di Serio, R. Tesser, Fluid-solid adsorption in batch and

continuous processing: a review and insights into modeling, Chem. Eng. Technol. 40 (2017) 799–820.
[54] V. Russo, R. Tesser, M. Trifuoggi, M. Giugni, M. Di Serio, A dynamic intraparticle model for fluid–solid adsorption kinetics, Comput. Chem. Eng. 74 (2015) 66–74.
[55] J. Zhou, S. Yang, J. Yu, Z. Shu, Novel hollow microspheres of hierarchical zinc–aluminum layered double hydroxides and their enhanced adsorption capacity for phosphate in water, J. Hazard. Mater. 192 (2011) 1114–1121.
[56] T. Prill, K. Schladitz, Simulation of FIB-SEM images for analysis of porous microstructures, Scanning 35 (2013) 189–195.
[57] A.B. Pribil, T.S. Hofer, B.R. Randolf, B.M. Rode, Structure and dynamics of phosphate ion in aqueous solution: an ab initio QMCF MD study, J. Comput. Chem. 29 (2008) 2330–2334.
[58] R.E. Beck, J.S. Schultz, Hindrance of solute diffusion within membranes as measured with microporous membranes of known pore geometry, Biochimica et Biophysica Acta (BBA) – Biomembranes 255 (1972) 273–303.